Synthesis of Aza-BODIPYs, Their Differential Binding for Cu(II), and Results of Bioimaging as Fluorescent Dyes of Langerhans β-Cells

Yaneth C. Pino, Jorge A. Aguilera, Víctor García-González, Manuel Alatorre-Meda,
Eustolia Rodríguez-Velázquez, Karla A. Espinoza, Héctor Frayde-Gómez, and Ignacio A. Rivero*
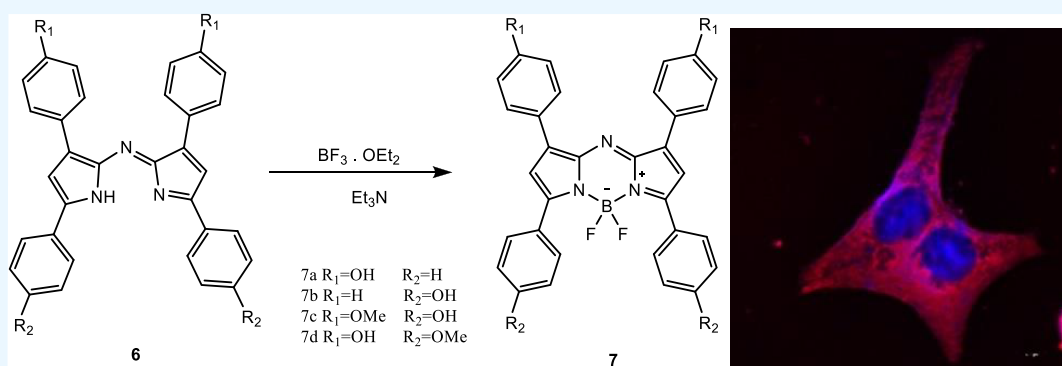
ACCESS | 📊 Metrics & More | 📰 Article Recommendations | 🗒 Supporting Information

ABSTRACT: Cellular labeling through the use of dyes is of great interest to the biomedical sciences for the characterization of the location and distribution of biomolecules and also for the tracking of the course of biological processes in both health and illness. This paper reports the synthesis, characterization, and subsequent evaluation as metal sensors and cell staining probes of four aza-BODIPY compounds [herein referred to as **7(a−d)**]. Compounds **7(b−d)** were found to display an outstanding selectivity for Cu(II) because their emission band at 720 nm was progressively quenched by this metal, presenting fluorescence quenching between 75 and 95%. On the other hand, cell imaging studies with pancreatic β-cells proved that aza-BODIPYs **7a** and **7b** showed selectivity for the cytoplasm, while **7c** and **7d** were selective for the cell membrane. Moreover, aza-BODIPY **7b** allowed to characterize in a clear way a lipotoxic condition mediated by saturated fatty acids, a critical phenomenon on β-cell damage associated with diabetes mellitus type II. Taken together, the presented results highlight the obtained aza-BODIPY compounds as selective sensing/staining probes with the potential to be used in the biomedical field.

1. INTRODUCTION

Diabetes mellitus types I and II are diseases that are characterized by hyperglycemia, resistance, and lack of insulin. The latter is due to the destruction of pancreatic islets; therefore, studies to determine the health of these cells are very important. The use of dyes to determine the status of Langerhans β-cells is very important to study the factors that affect their proliferation because these cells are responsible for the production of insulin required for the functions of the body.[1] Aza-BODIPY compounds are outstanding dyes that have been developed for cell characterization. These dyes have unique spectral properties such as intense absorption in the UV region, intense fluorescence, and high quantum yield. Moreover, these compounds are of great interest to many researchers because structural modifications modulate their optical properties such as fluorescence. In this context, synthesis and the exploration of their potential use in bioimaging, cancer therapy, and diagnosis have proven

important information for the design of novel aza-BODIPY photosensitizers for biomedical applications.[2−7]

The aza-BODIPY is obtained from the substitution of the *meso*-carbon atom (position 8) with one hydrogen atom. Nowadays, the development of fluorescent aza-BODIPY dyes has increased.[8−17] However, they have not been widely explored hitherto as fluorescent sensors.[12,18] According to the excellent characteristics described above, the aza-BODIPYs are recognized as molecules that offer a great opportunity to be used as fluorescent probes for organelle characterization, as well as in the evaluation of endocytosis.[11] In addition, aza-BODIPYs are good candidates for use in phototherapy because
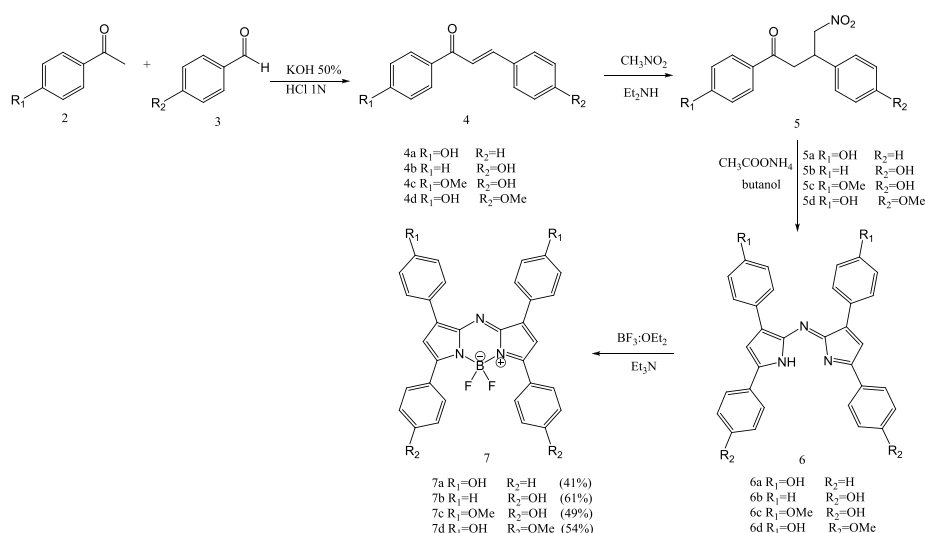
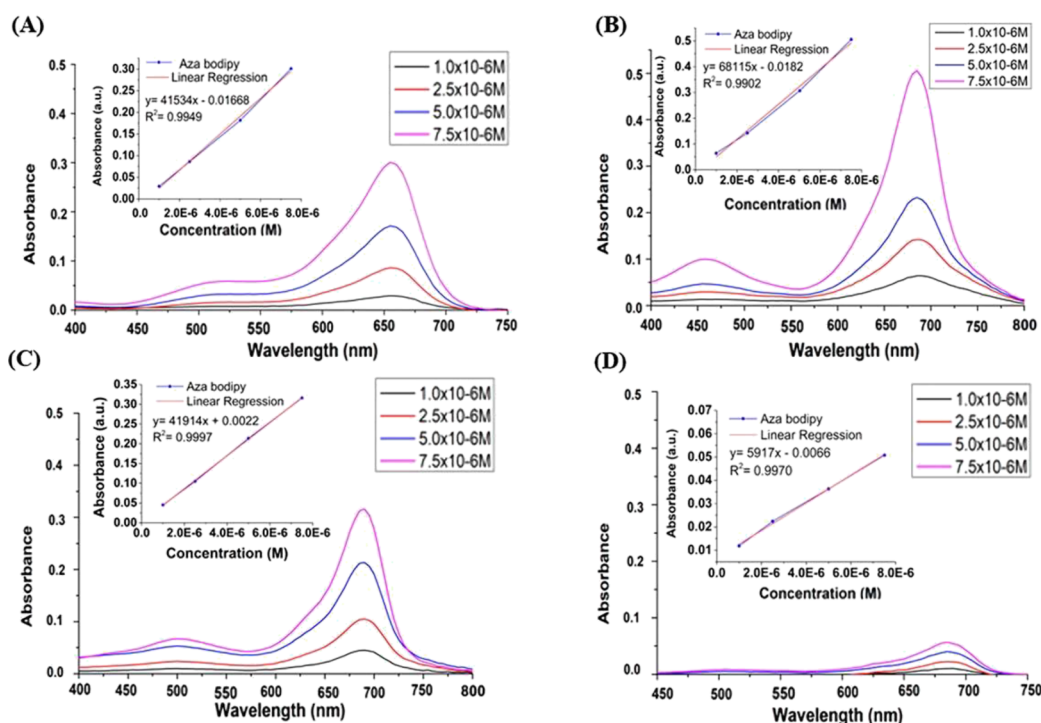**Figure 1.** Synthesis route for the four aza-BODIPY products. The chalcones (**4**) were condensed with nitromethane to obtain (**5**), which were reacted with ammonium acetate to obtain the dipyrrole imine groups (**6**), and finally with BF$_3$:Et$_2$O to obtain the aza-BODIPYs (**7**).

Figure 2. UV−vis absorption graphs of the aza-BODIPY compounds: (A) **7a**, (B) **7b**, (C) **7c**, and (D) **7d**. Insets in each graph show the linear regression of the absorption maxima with concentration.
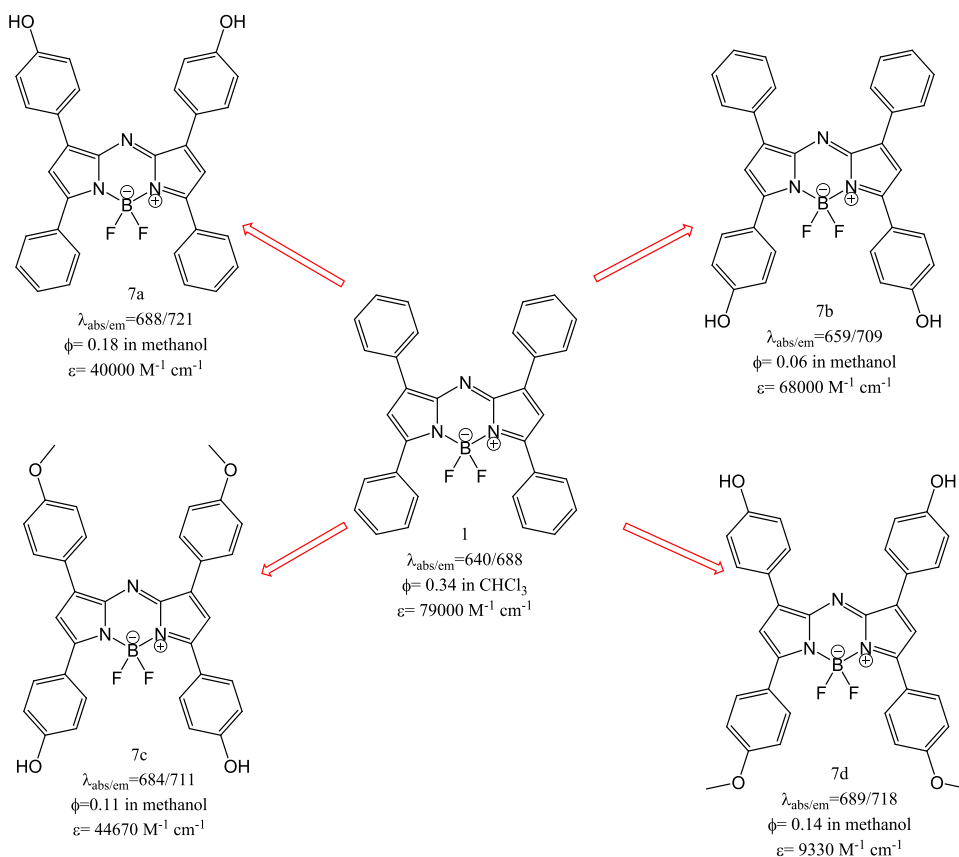
of their structural similarity to phthalocyanines. Phthalocyanines have already been tested for photodynamic therapy (PDT),[19,20] a soft and noninvasive technique that has been used in conjunction with medications for the successful treatment of several types of cancer.[20]

In this work, four aza-BODIPY compounds were synthesized and evaluated in terms of their photophysical properties, metal sensing by fluorescence quenching, and fluorescence staining of pancreatic Langerhans β-cells at healthy and induced lipotoxic conditions. The characterization was carried out by a battery of theoretical/experimental techniques including UV−vis and attenuated total reflectance−Fourier transform infrared spectroscopy (ATR−FTIR), ¹H and ¹⁹F NMR, mass

spectrometry, cell culture/staining, and confocal laser scanning microscopy (CLSM), among others.

2. RESULTS AND DISCUSSION

The selection of the aza-BODIPY as a molecule of interest relies on the fact that it is a fluorophore that when emitting at wavelengths greater than 700 nm allows a clear contrast against plenty of cell staining agents. Aza-BODIPYs are chemically stable and capable of penetrating the cytoplasm membrane with very little damage to the biological systems that are being studied when processing the images by fluorescence. Also, they present a high quantum yield.[12]

Scheme 1. Structures of the Synthesized Aza-BODIPY 7(a−d)[a]

7a
$\lambda_{abs/em}$=688/721
ϕ= 0.18 in methanol
ε= 40000 M^{-1} cm^{-1}

7b
$\lambda_{abs/em}$=659/709
ϕ= 0.06 in methanol
ε= 68000 M^{-1} cm^{-1}

1
$\lambda_{abs/em}$=640/688
ϕ= 0.34 in $CHCl_3$
ε= 79000 M^{-1} cm^{-1}

7c
$\lambda_{abs/em}$=684/711
ϕ=0.11 in methanol
ε= 44670 M^{-1} cm^{-1}

7d
$\lambda_{abs/em}$=689/718
ϕ= 0.14 in methanol
ε= 9330 M^{-1} cm^{-1}

[a]The red arrows indicate a bathochromic shift of the emission bands of each product relative to compound **1** whose photophysical properties were determined elsewhere.[22]
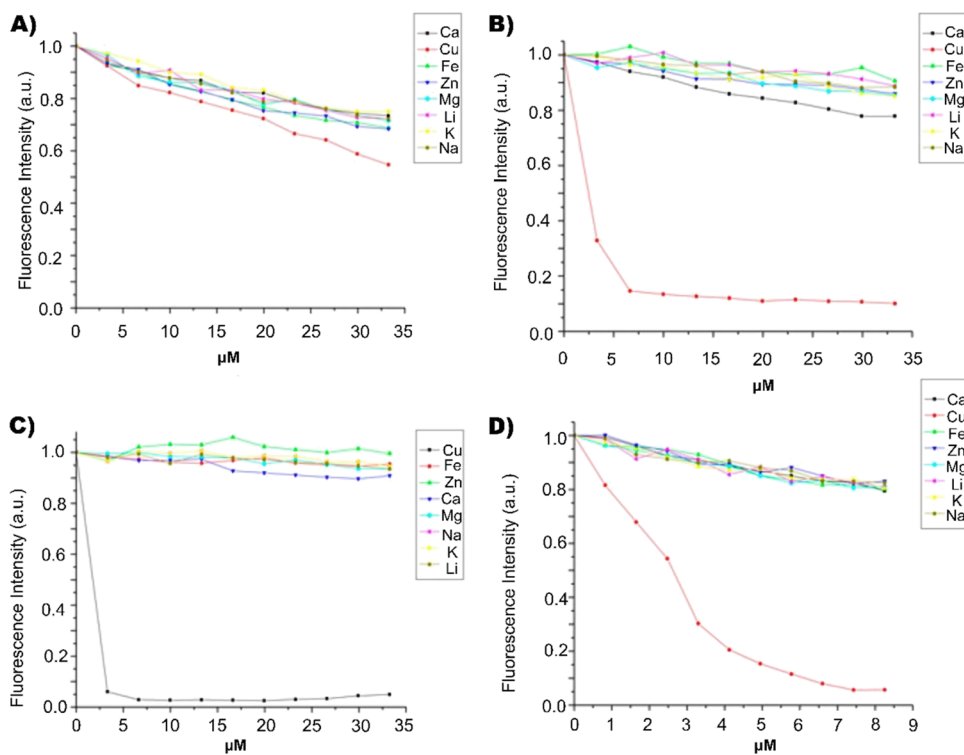
Figure 3. Fluorescence emission of aza-BODIPY compounds upon interaction with different metal ions: (A) **7a**, (B) **7b**, (C) **7c**, and (D) **7d**.
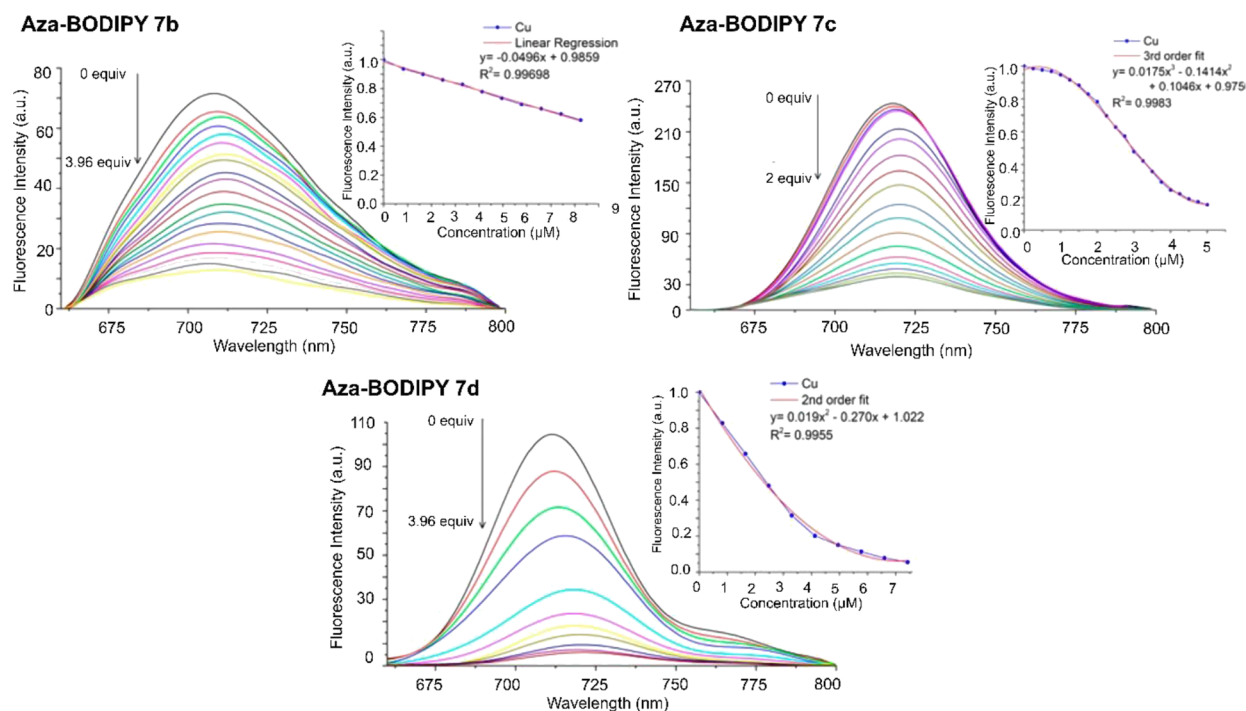
Figure 4. Fluorescence quenching of aza-BODIPY compounds with Cu(II) concentrations of 7.5×10^{-4} μM (**7b**), 7.5×10^{-4} μM (**7c**), and 10 μM (**7d**). Insets show the mathematical fitting of the experimental data.
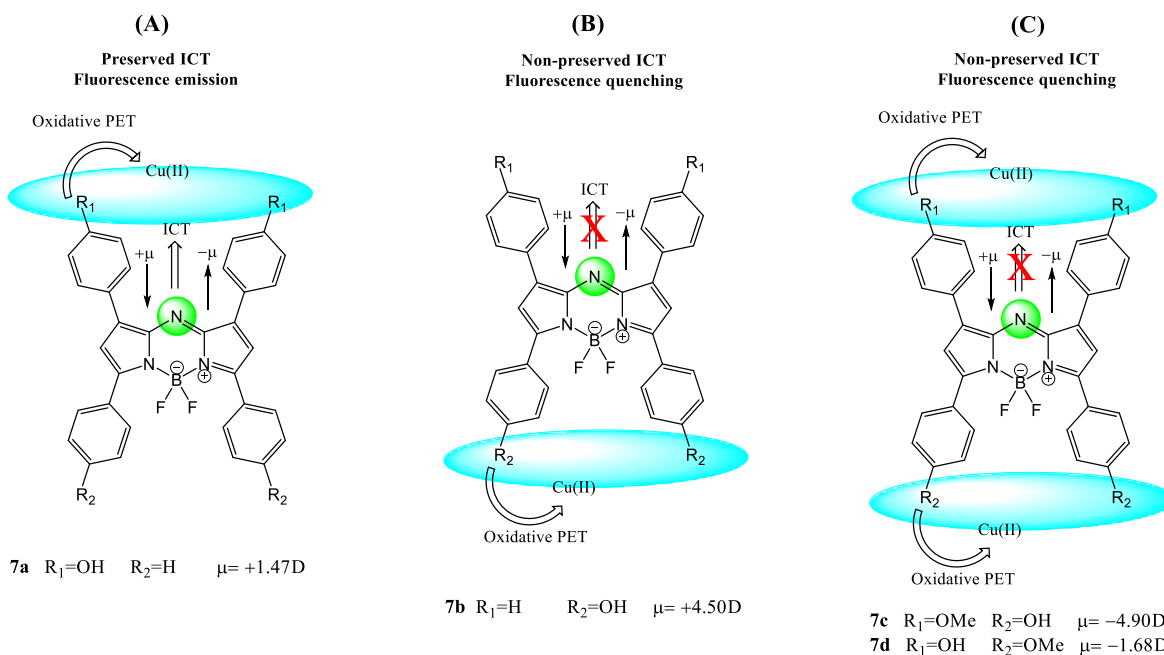

Figure 5. Proposed mechanism of the stablished aza-BODIPY:Cu(II) interactions and concomitant photophysical processes. Straight, small arrows denote the dipolar moment vectors (μ). Straight, empty arrows stand for the orientation of the expected ICT process. Red crosses denote the absence of the process. Green circles highlight the position of the nitrogen bridge (N8).

2.1. Synthesis of Aza-BODIPY.

The aza-BODIPY compounds (**7a**, **7b**, **7c**, and **7d**) were synthesized as described in Figure 1, starting with the Claisen-Schmidt condensation reaction of different acetophenones (**2**) and benzaldehydes (**3**) to obtain the corresponding chalcones (**4**) to subsequently carry out a Michael reaction with the addition of the nitro group in the β proton of the chalcone (**5**), followed by the synthesis to obtain the aza-dipyrromethenes (**6**) using ammonium acetate in butanol, which were finally reacted

with triethylamine and $BF_3 \cdot EtO_2$ for the synthesis of aza-BODIPYs (**7**).

2.2. Aza-BODIPY Spectroscopic Evaluation.

2.2.1. UV−Visible Spectroscopy. UV−vis experiments were performed to obtain the calibration curve of each aza-BODIPY with the following concentrations in acetonitrile 1×10^{-6}, 2.5×10^{-6}, 5.0×10^{-6}, and 7.5×10^{-6} M. Figure 2 shows the obtained results, presenting absorption bands at 655, 689, 688, and 684 nm for **7a**, **7b**, **7c**, and **7d**, respectively; the insets of each graph
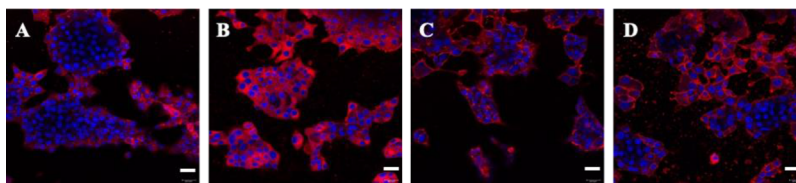
Figure 6. Cellular distribution of aza-BODIPY compounds on cultures of β-cells: (A) **7a**, (B) **7b**, (C) **7c**, and (D) **7d**. Hoechst 33342 was used as counterstain to identify the cell nuclei (blue staining). Scale bars stand for 20 μm.

show the linear regression of each absorption maxima as a function of concentration.

2.2.2. Fluorescence Spectroscopy. Scheme 1 shows the synthesized aza-BODIPY compounds **7(a−d)** containing protic (OH) and aprotic (−OCH₃) polar donor groups, their photophysical properties, and the effect of each group on their emission band relative to compound **1** (denoted by the red portrayed arrows). Fluorescence spectral data for all Aza-BODIPYs are summarized in Table S1, which also includes the calculation of quantum yields (Supporting Information).[21] In general, the emission maxima of all aza-BODIPYs were detected to occur within the 709−721 nm range, demonstrating a rather similar fluorescence response. As observed, the incorporation of oxygen induces a red shift of all compounds **7(a−d)** with respect to compound **1** and also modifies the quantum yield.[22] Interestingly, aza-BODIPY **7b** was found to present its absorption/emission bands at the shortest wavelengths (659/709 nm) and the largest Stokes shift (50 nm) (see Table S1). According to the literature, these changes are indicative of an intramolecular charge transfer (ICT) process between the aromatic rings at the 3,5-positions (donor) and the nitrogen bridge at the 8-position (N8, acceptor).[22] This ICT process is the key factor behind the fluorescence emission.[23]

As a next step in our study, we committed to characterize possible effects of the Li⁺, Na⁺, K⁺, Mg²⁺, Ca²⁺, Zn²⁺, Fe(III), and Cu(II) metal ions on the fluorescence emission of the aza-BODIPY compounds. These ions are of interest to the biomedical and environmental fields; the obtained results are shown in Figures 3 and 4. Figure 3A shows that aza-BODIPY **7a** is completely transparent to all ions under study, as evidenced by a mere slight decrease of the fluorescence signal with the metal concentration in all cases. By contrast, the rest of the aza-BODIPY compounds **7(b−d)** proved to present a high selectivity for the Cu(II) ion, as depicted by the sharp decrease of the fluorescence signal with Cu(II) concentration, nonobserved for the other metals (Figure 3B−D). Chemically speaking, aza-BODIPYs **7(b−d)** contain oxygen atoms in the methoxy and hydroxy groups positioned at the bottom of the structure in all cases (see Figure 1). In our opinion, this result reveals that these oxygen-bearing groups might promote quenching in the fluorescence signal by a competitive photo electron transfer oxidation process (PET) when interacting with the Cu(II) ion as a heavy atom, as discussed below. Interestingly, aza-BODIPY **7b** was found to present the greatest sensitivity for Cu(II) and very good linearity upon the metal titration (Figure 4). The fluorescence quenching of the aza-BODIPY **7b**:Cu(II) complex was determined to occur at a low Cu(II) concentration of 0.4 nM, proving to be lower than values previously reported for other systems.[24−29]

Figure 5 shows the possible driving mechanisms for the aza-BODIPY:Cu(II) interactions, which might explain the preservation or quenching of the fluorescence emission of

the aza-BODIPY products. In general, it appears that the presence and positions of oxygen atoms along the aza-BODIPY structure play a key role.

First, a photo electron transfer oxidation process (PET) is anticipated to occur with Cu(II) as it interacts with aza-BODIPY functional groups bearing oxygen atoms, as has been postulated in other similar models.[30] Next, the position of the oxygen atoms seems to govern a subsequent preservation or perturbance of the already stablished ICT process between the aromatic rings at the 3,5-positions (donor) and N8 (acceptor). Namely, the ICT process is preserved when the oxygen atoms are present in the 1,7-aromatic rings, thus keeping the fluorescence emission (see Figure 3, panel A). By contrast, when oxygen atoms are present in the 3,5-aromatic rings (see Figure 3, panels B and C), the ICT process is most likely perturbed by the oxidative PET process of Cu(II), which redistributes the electronic density of the aza-BODIPY:Cu(II) complex toward the Cu(II) ions in the opposite direction of the N8 atom, thereby quenching the fluorescence emission. This PET process is established between Cu(II) (acceptor) and oxygen (−OH and −OCH₃; donor),[30] making the Cu(II) ion to become paramagnetic while no interaction of Cu(II) with the nitrogen bridge (N8) is predicted because no increase in the fluorescence signal was observed.[31] In sum, the conjunction of these process is involved in the fluorescence quenching of the aza-BODIPY's compounds **7(b−d)** as they interact with Cu(II).[32]

Hartree−Fock calculations were carried out with the Gaussian 09 program to investigate, confirm, and support the driving mechanism of the binding between aza-BODIPY and Cu(II). Table S2 (Supporting Information) describes the performed calculations, including the dipole moments (μ) as well as the direction of the resulting vector. The obtained results demonstrated a fluctuation of μ for all aza-BODIPY compounds **7(a−d)**, from −4.90 to +4.50 Debye, and the resulting vector is directed toward positions 1 and 7, located on the nitrogen bridge (N8).[31] The effect of the oxygen atoms in the 3,5-positions when comparing structures **7a** and **7b** with compound **1** was that μ increased. In the particular case of structure **7b**, μ is greater than that in **7a**. The interaction of the Cu(II) cation with the aza-BODIPY strongly increases the μ of the latter structure and is clearly dependent on the position of the phenol groups. The difference in μ between base structure **1** and compounds **7(a−d)** denotes that the values are lower in polarity when having the hydroxy groups in the 1,7-positions and increase when they are in the 3,5-positions. The interaction of Cu(II) cations with the hydroxy of the 1,7-positions intensifies the magnitude of μ, with the resulting vector being oriented toward the nitrogen bridge (N8), but it does not promote the fluorescence quenching (**7a**); meanwhile, when interacting with the hydroxy groups of the rings at the 3,5-positions, the magnitude of μ increases in a similar proportion but obviously inverting its orientation. This
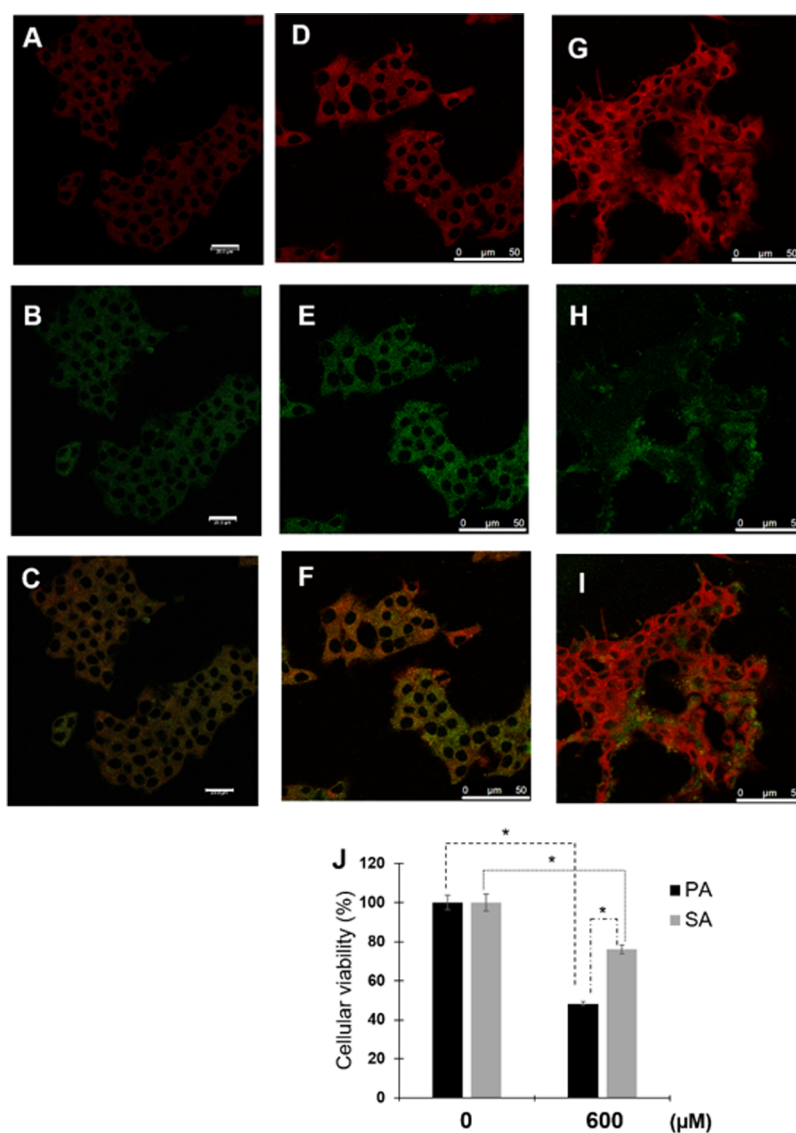
Figure 7. Aza-BODIPY **7b** colocalizes on endoplasmic reticulum and allows identifying Langerhans β-cell damage under lipotoxicity conditions. β-cells were incubated under the specific ER-probe, the ER-tracker (1 μM) (A), PA-BDP (25 μM) (B) and merge is showed (C). Scale bar in all images corresponds to 20 μm. Under the same PA-lipotoxicity induced, Aza-BODIPY **7b** was evaluated; cell images correspond to aza-BODIPY **7b** (0.8 μM) (D), PA-BDP (25 μM) (E), and merge (F). In a parallel way, SA-BDP was characterized; cell images correspond to aza-BODIPY **7b** (0.8 μM) (G), SA-BDP (25 μM) (H), and merge (I). As a complementary experimentation (J), lipotoxicity was characterized under standardized MTT assay (upon incubation for 20 h). The percentage of cell viability is shown. Mean values are presented ($n = 6$, mean ± SD), *$p < 0.01$.

observation is consistent with the fact that **7b** is the structure that presents the greatest decrease in the fluorescence signal when in contact with Cu(II).

2.2.3. Confocal Microscopy Analysis. In previous results of our group,[33,34] we characterized the role of lipotoxicity induced by free fatty acids on the deregulation of proteostasis of Langerhans β-cells (RIN-m5F cells), then in the control of their metabolism. Langerhans β-cells are well known as a model that maintains an active metabolism and insulin secretion. Having this in mind, we herein employed this cell line to evaluate the four synthesized aza-BODIPYs as staining agents. Results suggest a differential distribution of the products (Figure 6). Cell cultures treated with aza-BODIPYs **7c** and **7d** (0.4 μM) exhibited a membrane distribution of the probes (Figure 6A,C; red staining). Meanwhile, in the case of aza-BODIPYs **7a** and **7b**, the distribution was localized in the cytoplasm (Figure 6A,B), being more evident for aza-BODIPY

7b. Apparently, the presence of −OH groups in the aza-BODIPY structures favors their cytoplasmic localization of the probe, with greater efficiency in the case of compound **7b**. By contrast, the presence of the −OMe group in molecules **7c** and **7d** very likely promotes the impediment to permeabilize the cell membrane in the periphery of the cell clusters (Figure 6, panels A−E), leading to a preferential spatial ordering at the membrane level. Worth mentioning, the low concentration employed in this characterization (0.4 μM) highlights the aza-BODIPY products as having a high cell affinity. More micrographs at different magnifications can be found in the Supporting Information.

Considering the clear distribution of aza-BODIPY **7b** along the cytoplasm, the experimentation with this probe was extended to elucidate its localization and response at induced lipotoxic conditions, which are known to affect critical functions of Langerhans β-cells such as insulin secretion

(Figure 7).[33] Induced lipotoxicity and intracellular co-localization assays were carried out as reported previously,[33,34] employing fluorescent probes of palmitic (18C) and stearic acid (16C) coupled to BODIPY (PA-BDP and SA-BDP, respectively), along with commercial ER-tracker as a control (a fluorescent agent with high selectivity for the endoplasmic reticulum). We have identified PA and SA saturated fatty acids as inducers of endoplasmic reticulum stress, a phenomenon associated with alterations in insulin metabolism and cell toxicity.[33,34] The obtained results revealed that aza-BODIPY **7b** (red staining) co-localized indeed with ER-tracker, PA-BDP, and SA-BDP (all in green staining) on the endoplasmic reticulum, as evidenced by the red and green merge in the three cases (Figure 7; panels C, F, and I, respectively). As expected in these lipotoxic conditions, the cell viability was confirmed impaired upon incubation with PA and SA (Figure 7J).

Interestingly, these findings might be attractive for research in cell and molecular biology considering the already outlined affinity of aza-BODIPY **7b** for Cu(II) (see Figure 4B) and the well-known biological functions and localization of this metal at the intracellular level.[35,36] Copper is critical for the function of proteins involved in connective tissue formation, oxidative phosphorylation process, antioxidant mechanisms, and catecholamine synthesis.[37] For instance, ATP7A protein is a regulator of cell copper homeostasis, involving the supply of copper to copper-dependent enzymes within the *trans*-golgi network (TGN),[38,39] and copper efflux on the plasma membrane.[37] In an important way, several of these proteins are situated on the endoplasmic reticulum, highlighting the future exploration of these aza-BODIPY compounds as promising for the tracking of changes in Cu(II) levels at the cytoplasmic domain.

3. CONCLUSIONS

Four aza-BODIPY compounds containing protic (OH) and aprotic ($-OCH_3$) terminal groups (**7a−d**) were synthesized and characterized in terms of their photophysical properties, metal sensing by fluorescence quenching, and cell staining functionality in pancreatic Langerhans β-cells at healthy and induced lipotoxic conditions. Concerning their photophysical properties, all synthesized compounds presented a red shift in fluorescence emission and modified quantum yields relative to compound **1** (absent of terminal groups), with emission maxima in the 709−721 nm range. These changes were attributed to an ICT process most likely occurring between the aromatic rings at the 3,5-positions (donor) and the nitrogen bridge at the 8-position (N8, acceptor). On the other hand, with respect to metal sensing, aza-BODIPYs **7(b−d)** were found to present a high selectivity for the Cu(II) ion, as depicted by the sharp decrease of the fluorescence signal with Cu(II) concentration, nonobserved for the other metals under study (Li$^+$, Na$^+$, K$^+$, Mg^{2+}, Ca^{2+}, Zn^{2+}, Fe(III)). These compounds (**7b−d**) bear oxygen atoms in the methoxy and hydroxy terminal groups, positioned at the bottom of the structure in all cases, which might promote a quenching in the fluorescence signal by a competitive PET oxidation process when interacting with the Cu(II). Worth mentioning, The fluorescence quenching of the aza-BODIPY **7b**: Cu(II) complex was determined to occur at the low Cu(II) concentration of 0.4 nM (Figure 4B), proving to be lower than values previously reported for other systems. Finally, with respect to their cell staining functionality, it was verified that

the aza-BODIPYs **7(a, b)** selectively stained the cytoplasm, while aza-BODIPYs **7(c, d)** containing methoxy groups demonstrated a greater affinity to the cellular membrane. This finding suggests that the position of hydroxy and methoxy terminal groups plays a very important role in the cell affinity of the studied aza-BODIPY compounds. Taken together, the obtained results highlight the synthesized aza-BODIPY compounds as versatile cell staining agents with high selectivity for the cytoplasm and cell membrane, with additional capability of being sensitive for Cu(II) detection.

4. MATERIALS AND METHODS

4.1. General Procedures. All reagents and solvents were purchased from a commercial source (Sigma-Aldrich, Saint Louis, USA), and used without further purification. Anhydrous solvents for organics synthesis were prepared by passing through a solvent purification tower. Silica gel 60 (230−400 mesh) was used to purify the products. Thin-layer chromatography (TLC) was performed on silica gel F254 plates (Sigma-Aldrich, Saint Louis, USA). All compounds were detected using UV light. Melting points were obtained with an Electrothermal 88629 apparatus and were not corrected. Fourier transform infrared (FTIR) spectra were recorded with a PerkinElmer FTIR 1600 spectrometer. ^{1}H, ^{13}C, and ^{19}F nuclear magnetic resonance (NMR) spectra at 400, 101, and 376 MHz were recorded, respectively, using a Bruker Avance III spectrometer in CDCl$_3$, dimethyl sulfoxide (DMSO-d$_6$), or CD$_3$OD with tetramethylsilane (TMS) as an internal standard, and trifluoroacetic acid was the reference for ^{19}F spectra. Mass spectra were obtained with an Agilent Technologies 5975C MS spectrometer at 70 eV by direct insertion and an Agilent HPLC (Mod 1100) coupled to mass selective detector (MSD) version SL. High-resolution mass spectra (HRMS) were obtained with an Agilent ESI-QTOF (Mod G6530B). UV−vis absorption spectra were obtained with a Varian Cary 50 SCAN spectrophotometer. Fluorescence spectra were recorded with a Photon Technology International Fluorescence System with a 1 cm standard quartz cell.

4.2. General Method for Preparing Chalcones. In a 250 mL ball flask fitted with magnetic stirring, *p*-hydroxy acetophenone (5.0 g, 36.72 mmol) and benzaldehyde (3.73 mL, 36.72 mmol) in acetic acid (180 mL) were added and H$_2$SO$_4$ (6.0 mL) was gradually added. The reaction mixture is left for 12 h. The product (**4a**) was washed with distilled H$_2$O.

4.2.1. (E)-1-(4-Hydroxyphenyl)-3-phenylprop-2-en-1-one (4a). A red solid was obtained (1.2 g, 5.35 mmol, 69% yield). Mp 162−164 °C. IR (ATR, neat): 3105, 3060, 1644, 1599, 1562, 1442, 1283, 981 cm^{-1}. ^{1}H NMR (400 MHz, CDCl$_3$/DMSO-d$_6$): δ 10.42 (br, s, 1H), 8.09 (d, J = 8.0 Hz, 2H), 7.91 (d, J = 15.6 Hz, 1 H, β−H), 7.86 (m, 3H), 7.7 (d, J = 15.6 Hz, 1H, α-H), 7.4(dd, J_1 = 8.0 Hz, J_2 = 4.0 Hz, 2H), 6.93 (d, J = 8.0 Hz, 2H). ^{13}C NMR (101 MHz, CDCl$_3$/DMSO-d$_6$,): δ 187.8, 162.2, 142.9, 134.9130.8, 130.1, 129.4, 128.8, 128.2, 121.9, 115.5. ESI-MS m/z: C$_{15}$H$_{12}$O$_2$ found 222.71 (M−).

4.2.2. (E)-3-(4-Hydroxyphenyl)-1-phenylprop-2-en-1-one (4b). A red solid was obtained (1.66 g, 7.4 mmol, 89% yield). Mp 162−164 °C. IR (ATR, neat): 3200, 3057, 1643, 1577, 1349, 1211, 972 cm^{-1}. ^{1}H NMR (400 MHz, CDCl$_3$/DMSO-d$_6$): δ 10.1 (br, s, 1H), 8.1 (d, J = 8.0 Hz, 2H), 7.74 (d, J = 8.0 Hz, 2H), 7.89 (d, J = 15.6 Hz, 1 H, β-H), 7.64 (d, J = 8.0 Hz, 1H), 7.57 (d, J = 8.0 Hz, 2H), 7.53 (d, J = 15.6 Hz, 1H, α-H), 6.87 (d, J = 8.0 Hz, 2H). ^{13}C NMR (101 MHz, CDCl$_3$/

DMSO-d$_6$): δ 189.9, 160.4, 145.2, 138.5, 132.6, 130.4, 128.4, 128.0, 125.9, 118.5, 116.3. ESI-MS *m/z*: C$_{15}$H$_{12}$O$_2$ found 223.06 (M−).

4.2.3. (E)-3-(4-Hydroxyphenyl)-1-(4-methoxyphenyl)prop-2-en-1-one (4c). A pink solid was obtained (3.9 g, 11.8 mmol, 92% yield). Mp 170−172 °C. IR (neat): 3153, 3068, 1641, 1575, 1434.2, 1224, 1164, 1023, 827 cm^{-1}. ^{1}H NMR (400 MHz, CDCl$_3$/DMSO-d$_6$): δ 9.6 (br, s, 1H), 8.03 (d, *J* = 9.0 Hz, 2H), 7.72 (d, *J* = 15.6 Hz, 1H, *β*-H), 7.53 (d, *J* = 9.0 Hz, 2H), 7.43 (d, *J* = 15.6 Hz, 1H, *α*-H), 6.99 (d, *J* = 9.0 Hz, 2H), 6.88 (d, *J* = 9.0 Hz, 2H), 3.9 (s, H). ^{13}C NMR (101 MHz, CDCl$_3$/DMSO-d$_6$): δ 188.0, 163.1, 144.0, 131.1, 130.5, 130.3, 126.0, 118.3, 116.0, 113.7. ESI-MS *m/z*: C$_{16}$H$_{14}$O$_3$ found 252.62 (M−).

4.2.4. (E)-1-(4-Hydroxyphenyl)-3-(4-methoxyphenyl)prop-2-en-1-one (4d). A pink solid was obtained (1.2 g, 5.35 mmol, 73% yield). Mp 179−181 °C. IR (neat): 3153, 3068, 1641, 1575, 1434.2, 1224, 1164, 1023, 827 cm^{-1}. ^{1}H NMR (400 MHz, CDCl$_3$/DMSO-d$_6$): δ 9.88 (bs, 1H, OH), 7.96 (d, *J* = 8.0 Hz, 2H, Ar-H), 7.73 (d, *J* = 15.6 Hz, 1H, *β*-H), 7.61 (d, *J* = 8.0 Hz, 2H, Ar-H), 7.46 (d, *J* = 15.6 Hz, 1H, *α*-H), 6.93 (dd, *J*$_1$ = 8.0 Hz, *J*$_2$ = 2 Hz, 4H, Ar-H), 3.85 (s, 3H, methoxy). ^{13}C NMR (101 MHz, CDCl$_3$/DMSO-d$_6$): δ 194.0, 167.6, 167.0, 148.8, 136.4, 135.4, 133.2, 125.2, 120.1, 120.0, 119.8, 60.8. ESI-MS *m/z*: C$_{16}$H$_{14}$O$_3$ found 252.62 (M−).

4.3. General Method for Preparing Nitro Chalcones. In a 250 mL ball flask equipped with magnetic stirring, the chalcone (4a) (3.4 g, 14.9 mmol), CH$_3$NO$_2$ (4.0 mL, 74.56 mmol), and Et$_2$NH (7.7 mL) were added. The reaction mixture was maintained at a temperature of 60 °C for 15 h. It was kept at room temperature for half an hour and placed in a 250 mL separatory funnel, dissolved in ethyl acetate, and extractions were carried out with saturated NaCl (3 × 30 mL). The organic phase was dried with anhydrous Na$_2$SO$_4$; finally, the excess solvent was removed. Purification is carried out by flash chromatography using a mobile phase 7.0−3.0 petroleum ether−ethyl acetate.

4.3.1. 1-(4-Hydroxyphenyl)-4-nitro-3-phenylbutan-1-one (5a). Brown oil was obtained (3.0 g, 10.5 mmol, 70.0% yield). IR (ATR, neat): 3248.3, 1662.3, 1585.4, 1545.6, 1508.5, 1367.9, 1206.1, 834.8 cm^{-1}. ^{1}H NMR (400 MHz, CDCl$_3$/DMSO-d$_6$): δ 7.80 (d, *J*$_1$ = 8.0 Hz, 2H), 7.32−7.24 (m, 5H), 6.83 (d, *J*$_1$ = 8.0 Hz, 2H), 5.50 (bs, 1H), 4.72 (dddd, *J*$_1$ = 12.0 Hz, *J*$_2$ = 8.0 Hz 2H), 4.22−4.15 (m, 1H), 3.43−3.30 (m, 2H). ^{13}C NMR (101 MHz, CDCl$_3$/DMSO-d$_6$): δ 196.6, 161.4, 139.2, 130.8, 129.1, 127.9, 127.4, 115.7, 79.7, 41.2, 39.6 ppm. ESI-MS *m/z*: C$_{16}$H$_{15}$NO$_4$ found 283.72 (M−).

4.3.2. 3-(4-Hydroxyphenyl)-4-nitro-1-phenylbutan-1-one (5b). Brown oil was obtained (0.74 g, 2.6 mmol, 73.0% yield). IR (ATR, neat): 3375.7, 1678.2, 1593.4, 1545.6, 1450.1, 1375.9, 1206.1, 834.8 cm^{-1}. ^{1}H NMR (400 MHz, CDCl$_3$/DMSO-d$_6$): δ 7.90 (d, *J*$_1$ = 8.0 Hz, 2H), 7.56 (t, *J*$_1$ = 8.0 Hz, 1H), 7.44 (t, *J*$_1$ = 8.0 Hz, 2H), 7.09 (d, *J*$_1$ = 8.0 Hz, 2H), 6.73 (d, *J*$_1$ = 8.0 Hz, 2H), 6.08 (bs, 1H), 4.69 (dddd, *J*$_1$ = 12.0 Hz, *J*$_2$ = 8.0 Hz 1H), 4.1 (m, 2H), 3.41 (dd, *J*$_1$ = 8.0 Hz, *J*$_2$ = 4.0 Hz 2H). ^{13}C NMR (101 MHz, CDCl$_3$/DMSO-d$_6$): δ 197.7, 155.5, 136.4, 133.4, 130.6, 128.8, 128.1, 116.0, 79.9, 41.7, 38.8. ESI-MS *m/z*: C$_{16}$H$_{15}$NO$_4$ found 283.72 (M−).

4.3.3. 3-(4-Hydroxyphenyl)-1-(4-methoxyphenyl)-4-nitro-butan-1-one (5c). Brown oil was obtained (3.25 g, 10.31 mmol, 88.0% yield). IR (neat): 3341.1, 1654.4, 1596.0, 1513.8, 1442.2, 1264.5, 1163.7, 1031.1, 824.2 cm^{-1}. ^{1}H NMR (400 MHz, CDCl$_3$/DMSO-d$_6$): δ 7.88 (dd, *J*$_1$ = 8.0 Hz, *J*$_1$ =

4.0 Hz, 2H), 7.08 (dd, *J*$_1$ = 8.0 Hz, *J*$_1$ = 4.0 Hz, 2H), 6.91 (dd, *J*$_1$ = 8.0 Hz, *J*$_1$ = 4.0 Hz, 2H), 6.79 (dd, *J*$_1$ = 8.0 Hz, *J*$_1$ = 4.0 Hz, 2H), 4.87−4.54 (m, 2H), 4.17−402 (m, 2H), 3.86 (s, 3H), 3.44−319 (m, 1H). ^{13}C NMR (101 MHz, CDCl$_3$/DMSO-d$_6$): δ 195.7, 163.7, 156.7, 130.3, 129.8, 129.6, 128.4, 115.9, 113.8, 80.0, 55.5, 41.4, 38.9. ESI-MS *m/z*: C$_{17}$H$_{17}$NO$_5$ found 313.63 (M−).

4.3.4. 1-(4-Hydroxyphenyl)-3-(4-methoxyphenyl)-4-nitro-butan-1-one (5d). Brown oil was obtained (1.6 g, 5.1 mmol, 68.0% yield). IR (ATR, neat): 3277.5, 1662.3, 1601.3, 1585.4, 1511.1, 1436.9, 1248.6, 1163.7, 1025.8, 826.9 cm^{-1}. ^{1}H NMR (400 MHz, CDCl$_3$/DMSO-d$_6$): δ 7.82 (d, *J*$_1$ = 8.0 Hz, 2H), 7.17 (d, *J*$_1$ = 8.0 Hz, 2H), 6.93−6.74 (m, 4H), 4.69 (dddd, *J*$_1$ = 12.0 Hz, *J*$_2$ = 8.0 Hz 2H), 4.18−4.10 (m, 1H), 3.75 (s, 3H), 3.40−3.28 (m, 2H). ^{13}C NMR (101 MHz, CDCl$_3$/DMSO-d$_6$): δ 196.0, 161.2, 159.1, 131.1, 130.7, 129.3, 128.5, 115.6, 114.5, 79.9, 55.3, 41.3, 38.9. ESI-MS *m/z*: C$_{17}$H$_{17}$NO$_5$ found 313.76 (M−).

4.4. General Method for Preparing Aza-Dipyrromethenes. In a 250 mL ball flask equipped with magnetic stirring, nitro chalcone (5a) (1.2 g, 4.2 mmol) and CH$_3$COONH$_4$ (10.9 g, 141.4 mmol) in butanol (100 mL) were added. The reaction mixture was refluxed for 24 h. It was kept at room temperature for half an hour. The excess solvent was removed.

4.4.1. (Z)-4-(2-((5-(4-Hydroxyphenyl)-3-phenyl-1H-pyrrol-2-yl)imino)-3-phenyl-2H-pyrrol-5-yl)phenol (6a). A golden metallic solid was obtained (0.914 g, 1.7 mmol, 42.0% yield). Mp 274−276 °C. IR (ATR, neat): 3150.2, 1590.7, 1542.9, 1463.4, 1346.7, 1224.7, 906.4, 760.6 cm^{-1} ^{1}H NMR (400 MHz, CD$_3$COCD$_3$): δ 8.06 (d, *J* = 8.0 Hz, 4H), 7.86 (d, *J* = 8.6 Hz, 4H), 7.50−7.35 (m, 6H), 7.33 (s, 2H), 7.00 (d, *J* = 8.6 Hz, 4H). ^{13}C NMR (101 MHz, CD$_3$COCD$_3$): δ 160.1, 154.7, 149.1, 142.0, 134.0, 128.8, 128.5, 128.2, 127.7, 123.5, 116.3, 114.5. ESI-MS *m/z*: C$_{32}$H$_{23}$N$_3$O$_2$ found 480.02 (M−).

4.4.2. (Z)-4-(2-((3-(4-Hydroxyphenyl)-5-phenyl-1H-pyrrol-2-yl)imino)-5-phenyl-2H-pyrrol-3-yl)phenol (6b). A golden metallic solid was obtained (0.534 g, 0.98 mmol, 44.0% yield). Mp 320−322 °C. IR (neat): 3304.0, 1598.6, 1535.0, 1489.9, 1232.7, 898.5, 760.6 cm^{-1} ^{1}H NMR (400 MHz, CD$_3$COCD$_3$): δ 7.96 (d, *J* = 7.2 Hz, 4H), 7.92 (d, *J* = 8.8 Hz, 4H), 7.46 (t, *J* = 7.5 Hz, 3H), 7.38 (t, *J* = 7.3 Hz, 3H), 7.26 (s, 2H), 6.81 (d, *J* = 8.8 Hz, 4H). ^{13}C NMR (101 MHz, CD$_3$COCD$_3$): δ 157.9, 155.1, 149.3, 142.6, 132.2, 130.5, 130.1, 129.2, 126.5, 125.5, 115.3, 113.4. ESI-MS *m/z*: C$_{32}$H$_{23}$N$_3$O$_2$ found 480.25 (M+).

4.4.3. (Z)-4-(2-((3-(4-Hydroxyphenyl)-5-(4-methoxyphen-yl)-1H-pyrrol-2-yl)imino)-5-(4-methoxyphenyl)-2H-pyrrol-3-yl)phenol (6c). A golden metallic was obtained (0.712 g, 1.3 mmol, 47.0% yield). Mp 274−276 °C. IR (neat): 3330.6, 2839.9, 1598.7, 1497.8, 1460.8, 1243.3, 1023.1, 903, 792.0 cm^{-1}. ^{1}H NMR (400 MHz, CD$_3$COCD$_3$): δ 7.95 (d, *J* = 8.2 Hz, 8H), 7.30 (s, 2H), 7.2 (d, *J* = 8.8 Hz, 4H), 6.93 (d, *J* = 8.8 Hz, 4H), 3.90 (s, 6H). ^{13}C NMR (101 MHz, CD$_3$COCD$_3$): δ 162.4, 157.7, 150.8, 146.5, 141.7, 130.3, 128.1, 127.7, 123.0, 115.2, 114.8, 112.8, 55.0. ESI-MS *m/z*: C$_{34}$H$_{27}$N$_3$O$_4$ found 540.02 (M−).

4.4.4. (Z)-4-(2-((5-(4-Hydroxyphenyl)-3-(4-methoxyphen-yl)-1H-pyrrol-2-yl)imino)-3-(4-methoxyphenyl)-2H-pyrrol-5-yl)phenol (6d). A golden metallic solid was obtained (2.11 g, 3.8 mmol, 48.0% yield). Mp 260−262 °C. IR (ATR, neat): 3190.0, 2881.9, 1590.7, 1542.9, 1450.1, 1237.9, 1020.5, 898.5, 803.0 cm^{-1}. ^{1}H NMR (400 MHz, CD$_3$COCD$_3$): δ 8.18 (s, 2H), 7.95 (d, *J*$_1$ = 6.3 Hz, 8H), 7.3 (s, 2H), 7.2 (d, *J* = 8.1 Hz,

4H), 6.90 (d, J = 7.9 Hz, 4H), 3.90 (s, 6H). ^{13}C NMR (101 MHz, CD$_3$COCD$_3$): δ 164.6, 159.5, 155.6, 146.2, 131.1, 130.2, 128.3, 124.0, 116.2, 115.0, 113.7, 55.0. ESI-MS m/z: C$_{34}$H$_{27}$N$_3$O$_4$ found 540.04 (M−).

4.5. General Method for Preparing Aza-BODIPYs. Aza-dipyrromethene (**6a**) was added to a 50 mL ball flask equipped with magnetic stirring (0.08 g, 0.17 mmol), DIPEA (0.50 mL, 2.88 mmol), BF$_3$·OEt$_2$ (0.44 mL, 14.1 mmol), and DCM dry (15 mL) under inert conditions using argon. The reaction mixture was left in magnetic stirring at room temperature for 24 h. The excess solvent was removed to reduced pressure. The product was purified by prep-plate chromatography using a mobile phase of petroleum ether−ethyl acetate (7:3).

4.5.1. 4,4′-(5,5-Difluoro-3,7-diphenyl-5H-4λ4,5λ4-dipyrrolo[1,2-c:2′,1′-f][1,3,5,2]triazaborinine-1,9-diyl)-diphenol (7a).[40] Metallic solid red, (0.036 g, 0.07 mmol, 41.0% yield). Mp >330 °C. IR (ATR, neat): 3351.8, 1599.0, 1508.5, 1017.8, 816.3, 742.0 cm^{-1}. ^{1}H NMR (400 MHz, CD$_3$COCD$_3$): δ 8.20 (dd, J_1 = 17.4 Hz, J_2 = 8.0 Hz, 8H), 7.55−7.46 (m, 6H), 7.44 (s, 2H), 7.01 (d, J = 8.9 Hz, 4H). ^{13}C NMR (101 MHz, CD$_3$COCD$_3$): δ 160.2, 156.0, 145.1, 142.7, 133.1, 132.0, 130.1, 129.5, 128.0, 125.1, 118.2, 116.6. ^{19}F NMR (376 MHz, CD$_3$COCD$_3$): δ −131.93 (q, J = 36.0 Hz). ESI-MS m/z: C$_{32}$H$_{22}$BF$_2$N$_3$O$_2$ found 510.5 (M-H$_2$O-1).

4.5.2. 4,4′-(5,5-Difluoro-1,9-diphenyl-5H-4λ4,5λ4-dipyrrolo[1,2-c:2′,1′-f][1,3,5,2]triazaborinine-3,7-diyl)-diphenol (7b).[41] Metallic solid red, (0.038 g, 0.07 mmol, 61.0% yield). Mp >314 °C. IR (ATR, neat): 3370.3, 1604.0, 1582.8, 1484.6, 1227.4, 1025.8, 805.7, 742.0 cm^{-1}. ^{1}H NMR (400 MHz, CD$_3$COCD$_3$): δ 8.29−8.07 (m, 8H), 7.63−7.45 (m, 6H), 7.26 (s, 2H), 7.02 (d, J = 48.6 Hz, 4H). ^{13}C NMR (101 MHz, CD$_3$COCD$_3$): δ 160.4, 159.8, 146.1, 145.0, 133.0, 132.2, 131.5, 130.5, 129.3, 125.0, 118.3, 116.7. ^{19}F NMR (376 MHz, CD$_3$COCD$_3$): δ −130.29 (q, J = 32.0 Hz). ESI-MS m/z: C$_{32}$H$_{22}$BF$_2$N$_3$O$_2$ found 528.21 (M-1).

4.5.3. 4,4′-(5,5-Difluoro-1,9-bis(4-methoxyphenyl)-5H-4λ4,5λ4-dipyrrolo[1,2-c:2′,1′-f][1,3,5,2]triazaborinine-3,7-diyl)diphenol (7c).[42] Metallic solid red, (0.55 g, 0.93 mmol, 49.0% yield). Mp 218−220 °C. IR (ATR, neat): 3513.6, 3396.9, 1599.0, 1474.0, 1232.7, 1076.2, 813.6, 742.0 cm^{-1}. ^{1}H NMR (400 MHz, CD$_3$COCD$_3$): δ 8.9 (bs, 1H), 8.15 (dd, J_1 = 12.0 Hz, J_2 = 8.0 Hz, 8H), 7.25 (s, 2H), 7.07 (d, J = 8.0 Hz, 4H), 7.00 (d, J_1 = 8.0 Hz, 4H), 3.91 (s, 6H). ^{13}C NMR (101 MHz, CD$_3$COCD$_3$): δ 162.9, 158.6, 145.8, 143.9, 132.5, 131.9, 125.2, 125.1, 118.0, 116.6, 114.9, 55.9. ^{19}F NMR (376 MHz, CD$_3$COCD$_3$): δ −130.99 (q, J = 36.0 Hz). ESI-MS m/z: C$_{34}$H$_{26}$BF$_2$N$_3$O$_4$ found 588.28 (M−). HRMS (EI) m/z calcd for C$_{34}$H$_{26}$BF$_2$N$_3$NaO$_4$ [M] + 612.1877, found 612.1880.

4.5.4. 4,4′-(5,5-Difluoro-3,7-bis(4-methoxyphenyl)-5H-4λ4,5λ4-dipyrrolo[1,2-c:2′,1′-f][1,3,5,2]triazaborinine-1,9-diyl)diphenol (7d). Metallic solid red, (0.2 g, 0.33 mmol, 54.0% yield). Mp >252 °C. IR (ATR, neat): 3192.6, 1601.3, 1489.9, 1230.0, 1097.4, 805.7, 747.3 cm^{-1}. ^{1}H NMR (400 MHz, CD$_3$COCD$_3$): δ 8.20 (d, J = 9.0 Hz, 4H), 8.13 (d, J = 9.0 Hz, 4H), 7.29 (s, 2H), 7.10 (d, J = 9.0 Hz, 4H), 7.00 (d, J = 9.0 Hz, 4H), 3.90 (s, 6H). ^{13}C NMR (101 MHz, CD$_3$COCD$_3$): δ 161.9, 161.3, 145.0, 143.2, 132.8, 132.4, 131.7, 121.2, 124.2, 118.4, 115.1, 55.8. ^{19}F NMR (376 MHz, CD$_3$COCD$_3$): δ −131.22 (q, J = 32.0 Hz). ESI-MS m/z: C$_{34}$H$_{26}$BF$_2$N$_3$O$_4$ found 587.83 (M-1).

4.6. Computational Calculations. Hartree−Fock calculations were carried out with the Gaussian 09 program, employing the following conditions: RHF calculation method, 6-31G* basis set, charge 0, spin singlet.

Table S2 (Supporting Information) describes the performed calculations.

4.7. Cell Culture. In this study, a model of Langerhans β-cell was employed (RIN-m5F), and it comes from the American Type Cell Culture. RIN-m5F was proliferated in RPMI 1640 medium supplemented with glutamine and 10% fetal bovine serum. Penicillin (50 U/mL) and streptomycin (50 μg/L) were added to the media. The culture conditions were at a temperature of 37 °C and a 5% CO$_2$ humidified atmosphere, according to the previous protocols.[33,34,43]

4.8. Preparation of Fatty Acids. Models of lipotoxicity were evaluated according to previous work.[33,44] Palmitic (PA) and stearic acid (SA) were prepared in an ethanol/H$_2$O solution (1:1; vol:vol) at 60 °C to reach a final concentration of 75 mM. Subsequently, fatty acids (FA) were incubated with free FA-bovine serum albumin (BSA) for 2 h at 37 °C, filtered by 0.22 μm, and then diluted in a culture medium under different concentrations with a final molar ratio of 4:1 (FA/BSA),[16] before adding the different treatments to the culture plates.

4.9. Synthesis of BDP-FA. Based on a methodology developed by our group, BDP coupled to palmitic acid (BDP-PA) and BODIPY coupled to stearic acid (BDP-SA) were synthesized.[14] Briefly, BODIPY-8-ethylendiamine (0.436 mM) in dichloromethane anhydrous (8 mL) was added to N′-ethylcarbodiimide hydrochloride (0.524 mM), hydroxybenzotriazole (0.524 mm), N-methylmorpholine (1.308 mM), and the corresponding FA (0.48 mM). The mixture reaction was stirred for 5 h under the argon atmosphere at 25 °C. The solvent was eliminated under reduced pressure, and the product was dissolved in water (20 mL) and extracted with dichloromethane. The combined organic extracts were washed with brine and dried over anhydrous Na$_2$SO$_4$, and later, the product was concentrated. The crude product was purified by flash chromatography. All structures were confirmed by mass spectroscopy and nuclear magnetic resonance (NMR).

4.10. Confocal Microscopy. A LEICA TCS-SP8 confocal laser scanning microscope (LEICA Microsystems Heidelberg GmbH) was employed to characterize the cellular distribution of the Aza-BODIPYs under different metabolic overload conditions. For these experiments, cells were proliferated to reach 90% of confluence on glass coverslips, previously treated with UV radiation for 30 min. Then, during 1 h, cells were maintained in starving conditions without PBS and treated under different experimental conditions. Later, cell cultures were washed with PBS three times, incubated with aza-BODIPY (**7b**) for 30 min (0.8 μM), and then, the Hoechst probe was added to the cultures and incubated for 30 min. Later, cells were washed extensively and fixed with cold paraformaldehyde and mounted for observation. Macroscopically different zones were recorded, preferentially at the center of the specimens, to depict representative images. Images were recorded at excitation/emission wavelengths of 405/430−550 and 638/650−750 nm for the detection of Hoechst (blue) and aza-BODIPY (**7b**) (red), respectively.

4.10.1. Colocalization of the ER-Tracker Probe and BDP-FA. RIN-m5F cells were proliferated to 90% of confluence and treated with BDP-PA and SA (5−25 μM) for 12 h. Later, culture cells were washed with HBSS buffer, and then, ER-tracker (1 μM) was added and incubated for 25 min at 37 °C. ER-tracker is a fluorescent probe that colocalizes on

endoplasmic reticulum. Cells were washed once with HBSS buffer and fixed with 4% formaldehyde for 2 min at 37 °C. Finally, cells were washed twice with PBS 1×. Images were recorded at excitation/emission wavelengths of 488/495−545 and 587/615 nm for the detection of BDP-PA, BDP-SA (green), and ER-tracker (red), respectively.

4.11. Cell Viability Assays. Cell viability was evaluated using the MTT assay according to previous protocols of our group.[45]

First, cells were seeded onto 96-well plates at a density of 23,000 cells/well and allowed to grow at 90% of confluence. Next, the culture medium was replaced with an Opti-MEM medium. After 2 h under this condition, cells were treated under the desired experimental conditions. Later, 30 μL of an MTT stock solution (2.1 mg/mL) was added to the culture media to obtain a final concentration of 0.5 mg/mL. Formazan crystals formed after 4 h of incubation were further dissolved by adding buffer lysis (20% sodium dodecyl sulfate, 50% N,N-dimethylformamide, pH 4.0). Finally, the optical density was measured at 570 nm using a microplate reader. Data are expressed as mean $\pm$ SD.

4.12. Statistical Analysis. Statistical analyses were conducted by the one-way analysis of variance (ANOVA) protocol, and differences among means were compared with the Bonferroni assay using a significance level of $p < 0.01$.

■ ASSOCIATED CONTENT

SI Supporting Information

The Supporting Information is available free of charge at https://pubs.acs.org/doi/10.1021/acsomega.2c04151.

> The included file contains the following results: ^{1}H NMR, ^{13}C NMR, ^{19}F NMR, FTIR, UV−vis, MF, MS, and HRMS spectra; microscopy confocal images; and the results of theoretical calculations of aza-BODIPYs (PDF)

■ AUTHOR INFORMATION

Corresponding Author

Ignacio A. Rivero − Centro de Graduados e Investigación en Química, Tecnológico Nacional de México/Instituto Tecnológico de Tijuana, Tijuana, BC 22510, México; ● orcid.org/0000-0003-4920-6379; Email: irivero@ tectijuana.mx

Authors

Yaneth C. Pino − Centro de Graduados e Investigación en Química, Tecnológico Nacional de México/Instituto Tecnológico de Tijuana, Tijuana, BC 22510, México

Jorge A. Aguilera − Centro de Graduados e Investigación en Química, Tecnológico Nacional de México/Instituto Tecnológico de Tijuana, Tijuana, BC 22510, México

Víctor García-González − Departamento de Bioquímica, Facultad de Medicina Mexicali, Universidad Autónoma de Baja California, Mexicali, BC 21100, México

Manuel Alatorre-Meda − Centro de Graduados e Investigación en Química-Grupo de Biomateriales y Nanomedicina, CONACyT-Tecnológico Nacional de México/Instituto Tecnológico de Tijuana, Tijuana, BC 22510, México; ● orcid.org/0000-0002-3301-9619

Eustolia Rodríguez-Velázquez − Facultad de Odontología, Universidad Autónoma de Baja California, Tijuana, BC 22390, México; Centro de Graduados e Investigación en Química-Grupo de Biomateriales y Nanomedicina, Tecnológico Nacional de México/Instituto Tecnológico de Tijuana, Tijuana, BC 22510, México

Karla A. Espinoza − Centro de Graduados e Investigación en Química, Tecnológico Nacional de México/Instituto Tecnológico de Tijuana, Tijuana, BC 22510, México

Héctor Frayde-Gómez − Departamento de Bioquímica, Facultad de Medicina Mexicali, Universidad Autónoma de Baja California, Mexicali, BC 21100, México

Complete contact information is available at:
https://pubs.acs.org/10.1021/acsomega.2c04151

Notes

The authors declare no competing financial interest.

■ ACKNOWLEDGMENTS

■ REFERENCES

(1) Ávila-Cossío, M. E.; Rivero, I. A.; García-González, V.; Alatorre-Meda, M.; Rodríguez-Velázquez, E.; Calva-Yáñez, J. C.; Espinoza, K. A.; Pulido-Capiz, Á. Preparation of Polymeric Films of PVDMA-PEI Functionalized with Fatty Acids for Studying the Adherence and Proliferation of Langerhans β-Cells. ACS Omega 2020, 5, 5249−5257.

(2) Zhang, T.; Ma, C.; Sun, T.; Xie, Z. Unadulterated BODIPY Nanoparticles for Biomedical Applications. Coord. Chem. Rev. 2019, 390, 76−85.

(3) Kolemen, S.; Akkaya, E. U. Reaction-Based BODIPY Probes for Selective Bio-Imaging. Coord. Chem. Rev. 2018, 354, 121−134.

(4) Konken, C. P.; Haufe, G.; Brömmel, K.; Wünsch, B.; Schäfers, M.; Wagner, S.; Hugenberg, V. Development of Symmetric O-BODIPYs with Different Optical Properties as Building Blocks for the Synthesis of Ligands for Multimodal Imaging. Dyes Pigm. 2018, 158, 88−96.

(5) Bertrand, B.; Passador, K.; Goze, C.; Denat, F.; Bodio, E.; Salmain, M. Metal-Based BODIPY Derivatives as Multimodal Tools for Life Sciences. Coord. Chem. Rev. 2018, 358, 108−124.

(6) Kue, C. S.; Ng, S. Y.; Voon, S. H.; Kamkaew, A.; Chung, L. Y.; Kiew, L. V.; Lee, H. B. Recent Strategies to Improve Boron Dipyrromethene (BODIPY) for Photodynamic Cancer Therapy: An Updated Review. Photochem. Photobiol. Sci. 2018, 17, 1691−1708.

(7) Ni, Y.; Wu, J. Far-Red and near Infrared BODIPY Dyes: Synthesis and Applications for Fluorescent PH Probes and Bio-Imaging. Org. Biomol. Chem. 2014, 12, 3774−3791.

(8) Loudet, A.; Burgess, K. BODIPY Dyes and Their Derivatives: Syntheses and Spectroscopic Properties. Chem. Rev. 2007, 107, 4891−4932.

(9) Loudet, A.; Bandichhor, R.; Wu, L.; Burgess, K. Functionalized BF2 Chelated Azadipyrromethene Dyes. Tetrahedron 2008, 64, 3642−3654.

(10) Bandodkar, A. J.; Wang, J. Non-Invasive Wearable Electrochemical Sensors: A Review. Trends Biotechnol. 2014, 32, 363−371.

(11) Zhao, W.; Carreira, E. M. Conformationally Restricted Aza-BODIPY: Highly Fluorescent, Stable Near-Infrared Absorbing Dyes. Chem. — Eur. J. 2006, 12, 7254−7263.

(12) Gorman, A.; Killoran, J.; O'Shea, C.; Kenna, T.; Gallagher, W. M.; O'Shea, D. F. In Vitro Demonstration of the Heavy-Atom Effect

for Photodynamic Therapy. *J. Am. Chem. Soc.* **2004**, *126*, 10619−10631.

(13) McDonnell, S. O.; Hall, M. J.; Allen, L. T.; Byrne, A.; Gallagher, W. M.; O'Shea, D. F. Supramolecular Photonic Therapeutic Agents. *J. Am. Chem. Soc.* **2005**, *127*, 16360−16361.

(14) Hall, M. J.; Allen, L. T.; O'Shea, D. F. PET Modulated Fluorescent Sensing from the BF2 Chelated Azadipyrromethene Platform. *Org. Biomol. Chem.* **2006**, *4*, 776−780.

(15) Kamkaew, A.; Thavornpradit, S.; Puangsamlee, T.; Xin, D.; Wanichacheva, N.; Burgess, K. Oligoethylene Glycol-Substituted Aza-BODIPY Dyes as Red Emitting ER-Probes. *Org. Biomol. Chem.* **2015**, *13*, 8271−8276.

(16) McDonnell, S. O.; O'Shea, D. F. Near-Infrared Sensing Properties of Dimethlyamino-Substituted BF2-Azadipyrromethenes. *Org. Lett.* **2006**, *8*, 3493−3496.

(17) Coskun, A.; Yilmaz, M. D.; Akkaya, E. U. Bis(2-Pyridyl)-Substituted Boratriazaindacene as an NIR-Emitting Chemosensor for Hg(II). *Org. Lett.* **2007**, *9*, 607−609.

(18) Killoran, J.; Allen, L.; Gallagher, J. F.; Gallagher, W. M.; O'Shea, D. F. Synthesis of BF2 Chelates of Tetraarylazadipyrromethenes and Evidence for Their Photodynamic Therapeutic Behaviour. *Chem. Commun.* **2002**, *17*, 1862−1863.

(19) Lopez, T.; Ortiz, E.; Alvarez, M.; Navarrete, J.; Odriozola, J. A.; Martinez-Ortega, F.; Páez-Mozo, E. A.; Escobar, P.; Espinoza, K. A.; Rivero, I. A. Study of the Stabilization of Zinc Phthalocyanine in Sol-Gel TiO$_2$ for Photodynamic Therapy Applications. *Nanomedicine* **2010**, *6*, 777.

(20) Dolmans, D. E. J. G. J.; Fukumura, D.; Jain, R. K. Photodynamic Therapy for Cancer. *Nat. Rev. Cancer* **2003**, *3*, 380−387.

(21) Zhang, X. F.; Zhang, Y.; Liu, L. Fluorescence Lifetimes and Quantum Yields of Ten Rhodamine Derivatives: Structural Effect on Emission Mechanism in Different Solvents. *J. Lumin.* **2014**, *145*, 448−453.

(22) Shi, Z.; Han, X.; Hu, W.; Bai, H.; Peng, B.; Ji, L.; Fan, Q.; Li, L.; Huang, W. Bioapplications of Small Molecule Aza-BODIPY: From Rational Structural Design to in Vivo Investigations. *Chem. Soc. Rev.* **2020**, *49*, 7533−7567.

(23) Ma, D.; Hou, S.; Bae, C.; Pham, T. C.; Lee, S.; Zhou, X. Aza-BODIPY Based Probe for Photoacoustic Imaging of ONOO− in Vivo. *Chin. Chem. Lett.* **2021**, *32*, 3886−3889.

(24) Vopálenská, I.; Váchová, L.; Palková, Z. New Biosensor for Detection of Copper Ions in Water Based on Immobilized Genetically Modified Yeast Cells. *Biosens. Bioelectron.* **2015**, *72*, 160−167.

(25) Sun, S.; Wu, X.; Huang, Y.; Jiang, Q.; Zhu, S.; Sun, S. Visual Detection of Cu^{2+} in High-Copper Feed Based on a Fluorescent Derivative of Rhodamine B. *Microchem. J.* **2021**, *171*, No. 106858.

(26) Ren, M.; Xu, Q.; Bai, Y.; Wang, S.; Kong, F. Construction of a Dual-Response Fluorescent Probe for Copper (II) Ions and Hydrogen Sulfide (H2S) Detection in Cells and Its Application in Exploring the Increased Copper-Dependent Cytotoxicity in Present of H2S. *Spectrochim. Acta, Part A* **2021**, *249*, No. 119299.

(27) Durgadas, C. V.; Sharma, C. P.; Sreenivasan, K. Fluorescent Gold Clusters as Nanosensors for Copper Ions in Live Cells. *Analyst* **2011**, *136*, 933−940.

(28) Liu, M.; Wang, K.; Wang, H.; Lu, J.; Xu, S.; Zhao, L.; Wang, X.; Du, J. Simple and Sensitive Colorimetric Sensors for the Selective Detection of Cu(II). *RSC Adv.* **2021**, *11*, 11732−11738.

(29) Saleh, S. M.; Ali, R.; Alminderej, F.; Ali, I. A. I. Ultrasensitive Optical Chemosensor for Cu(II) Detection. *Int. J. Anal. Chem.* **2019**, *2019*, 1.

(30) Xie, X.; Qin, Y. A Dual Functional near Infrared Fluorescent Probe Based on the Bodipy Fluorophores for Selective Detection of Copper and Aluminum Ions. *Sens. Actuators, B* **2011**, *156*, 213−217.

(31) Gawale, Y.; Mangalath, S.; Adarsh, N.; Joseph, J.; Ramaiah, D.; Sekar, N. Novel Aza-BODIPY Based Turn on Selective and Sensitive Probe for on-Site Visual Detection of Bivalent Copper Ions. *Dyes Pigm.* **2019**, *171*, No. 107684.

(32) Praikaew, P.; Roongcharoen, T.; Charoenpanich, A.; Kungwan, N.; Wanichacheva, N. Near-IR Aza-BODIPY-Based Probe for the Selective Simultaneous Detection of Cu^{2+} in Aqueous Buffer Solutions and Its Application in Biological Samples. *J. Photochem. Photobiol., A* **2020**, *400*, No. 112641.

(33) Acosta-Montaño, P.; Rodríguez-Velázquez, E.; Ibarra-López, E.; Frayde-Gómez, H.; Mas-Oliva, J.; Delgado-Coello, B.; Rivero, I. A.; Alatorre-Meda, M.; Aguilera, J.; Guevara-Olaya, L.; García-González, V. Fatty Acid and Lipopolysaccharide Effect on Beta Cells Proteostasis and Its Impact on Insulin Secretion. *Cell* **2019**, *8*, 884.

(34) Pulido-Capiz, A.; Díaz-Molina, R.; Martínez-Navarro, I.; Guevara-Olaya, L. A.; Casanueva-Pérez, E.; Mas-Oliva, J.; Rivero, I. A.; García-González, V. Modulation of Amyloidogenesis Controlled by the C-Terminal Domain of Islet Amyloid Polypeptide Shows New Functions on Hepatocyte Cholesterol Metabolism. *Front. Endocrinol.* **2018**, *9*, 331.

(35) Acosta-Montaño, P.; García-González, V. Effects of Dietary Fatty Acids in Pancreatic Beta Cell Metabolism, Implications in Homeostasis. *Nutrients* **2018**, *10*, 393.

(36) García-González, V.; Gutiérrez-Quintanar, N.; Mas-Oliva, J. The C-Terminal Domain Supports a Novel Function for CETPI as a New Plasma Lipopolysaccharide-Binding Protein. *Sci. Rep.* **2015**, *5*, 16091.

(37) Prohaska, J. R.; Gybina, A. A. Intracellular Copper Transport in Mammals. *J. Nutr.* **2004**, *134*, 1003−1006.

(38) Petris, M. J.; Mercer, J. F. B.; Culvenor, J. G.; Lockhart, P.; Gleeson, P. A.; Camakaris, J. Ligand-Regulated Transport of the Menkes Copper P-Type ATPase Efflux Pump from the Golgi Apparatus to the Plasma Membrane: A Novel Mechanism of Regulated Trafficking. *EMBO J.* **1996**, *15*, 6084−6095.

(39) Yamaguchi, Y.; Heiny, M. E.; Suzuki, M.; Gitlin, J. D. Biochemical Characterization and Intracellular Localization of the Menkes Disease Protein. *Proc. Natl. Acad. Sci. U. S. A.* **1996**, *93*, 14030−14035.

(40) Bandi, V.; El-Khouly, M. E.; Ohkubo, K.; Nesterov, V. N.; Zandler, M. E.; Fukuzumi, S.; D'Souza, F. Excitation-Wavelength-Dependent, Ultrafast Photoinduced Electron Transfer in Bisferrocene/BF2-Chelated-Azadipyrromethene/Fullerene Tetrads. *Chem. − Eur. J.* **2013**, *19*, 7221−7230.

(41) Xu, J.; Zhai, J.; Xu, Y.; Zhu, J.; Qin, Y.; Jiang, D. A Near-Infrared Fluorescent Aza-Bodipy Probe for Dual-Wavelength Detection of Hydrogen Peroxide in Living Cells. *Analyst* **2016**, *141*, 2380−2383.

(42) Xiang, H. J.; Tham, H. P.; Nguyen, M. D.; Fiona Phua, S. Z.; Lim, W. Q.; Liu, J. G.; Zhao, Y. An Aza-BODIPY Based near-Infrared Fluorescent Probe for Sensitive Discrimination of Cysteine/Homocysteine and Glutathione in Living Cells. *Chem. Commun.* **2017**, *53*, 5220−5223.

(43) Martínez-Navarro, I.; Díaz-Molina, R.; Pulido-Capiz, A.; Mas-Oliva, J.; Luna-Reyes, I.; Rodríguez-Velázquez, E.; Rivero, I. A.; Ramos-Ibarra, M. A.; Alatorre-Meda, M.; García-González, V. Lipid Modulation in the Formation of β-Sheet Structures. Implications for De Novo Design of Human Islet Amyloid Polypeptide and the Impact on β-Cell Homeostasis. *Biomolecules* **2020**, *10*, 1−21.

(44) Galindo-Hernández, O.; Córdova-Guerrero, I.; Díaz-Rubio, L. J.; Pulido-Capiz, Á.; Díaz-Villanueva, J. F.; Castañeda-Sánchez, C. Y.; Serafín-Higuera, N.; García-González, V. Protein Translation Associated to PERK Arm Is a New Target for Regulation of Metainflammation: A Connection with Hepatocyte Cholesterol. *J. Cell. Biochem.* **2019**, *120*, 4158−4171.

(45) García-González, V.; Mas-Oliva, J. Amyloidogenic Properties of a D/N Mutated 12 Amino Acid Fragment of the C-Terminal Domain of the Cholesteryl-Ester Transfer Protein (CETP). *Int. J. Mol. Sci.* **2011**, *12*, 2019−2035.